

## Supporting Information

### MXenes as Thermal Catalysts. Nb<sub>2</sub>C Mxene as Bifunctional Acid-Base and Oxidation/Hydrogenation Catalyst

Octavian Pavel,<sup>a</sup> Alina Tirsoaga,<sup>a</sup> Bogdan Cojocaru,<sup>a</sup> Dana Popescu,<sup>a</sup> Ruben Ramírez-Grau,<sup>b</sup> Pablo González-Durán<sup>b</sup>, Pablo García-Aznar<sup>b</sup>, Liang Tian<sup>b</sup>, Germán Sastre,<sup>b</sup> Ana Primo,<sup>b,\*</sup> Vasile Parvulescu,<sup>a,\*</sup> Hermenegildo Garcia<sup>b</sup>

<sup>a</sup>Department of Organic Chemistry, Biochemistry and Catalysis, Faculty of Chemistry, University of Bucharest, Bdul Regina Elisabeta 4-12, Bucharest 030016, Romania

**E-mail:** [vasile.parvulescu@chimie.unibuc.ro](mailto:vasile.parvulescu@chimie.unibuc.ro)

<sup>b</sup> Instituto Universitario de Tecnología Química, Consejo Superior de Investigaciones Científicas-Universitat Politecnica de Valencia, Universitat Politecnica de Valencia, Av. De los Naranjos s/n, 46022 Valencia, Spain. **E-mail:** [aprimoar@itq.upv.es](mailto:aprimoar@itq.upv.es)

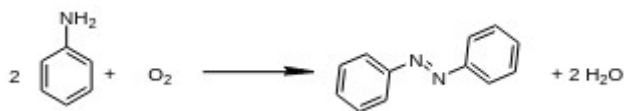
#### Index

Aniline coupling to give azobenzene on Nb <sub>2</sub> CO <sub>2</sub> Mxene. Computational study.....	S3
XPS data of the Nb <sub>2</sub> C sample after being used as catalysts.....	S4
Computational methods.....	S5
Computational models.....	S7
Computational results.....	S8
Geometry optimization of Nb <sub>2</sub> CO <sub>2</sub> MXene.....	S7
Geometry optimization of all the reaction steps of the aniline coupling.....	S8
Step 1.....	S9
Step 2.....	S10
Step 3.....	S11
Step 4.....	S11
Step 5.....	S12
Step 6.....	S12
Step 7.....	S13
Step 8.....	S13
Step 9.....	S14
Step 10.....	S14
Step 11.....	S15
Step 12.....	S15

Synergy between Matlantis and CASTEP.....S16

### Aniline coupling to give azobenzene on Nb<sub>2</sub>CO<sub>2</sub> MXene. Computational study.

Azobenzene can be synthesized, among other routes, by oxidative coupling of anilines. The overall reaction of the process involves 2 molecules of aniline and 1 molecule of oxygen as oxidant, obtaining azobenzene and two molecules of water, as indicated in the following equation



**Equation S1.** Global reaction scheme of aniline coupling to give azobenzene.

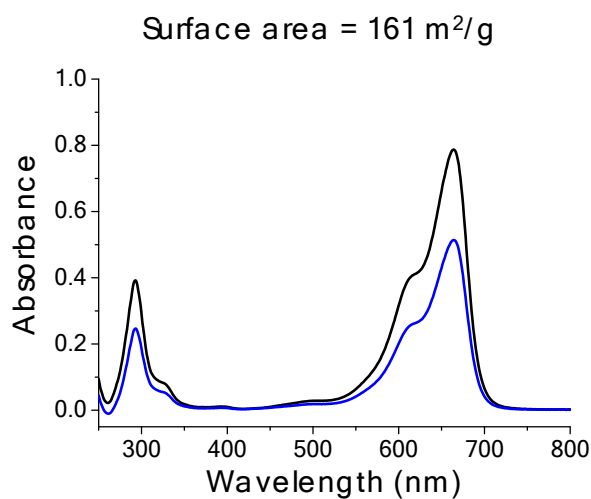


**Fig. S1.** Surface area of Nb<sub>2</sub>C suspended in H<sub>2</sub>O based on the decrease on methylene blue concentration.

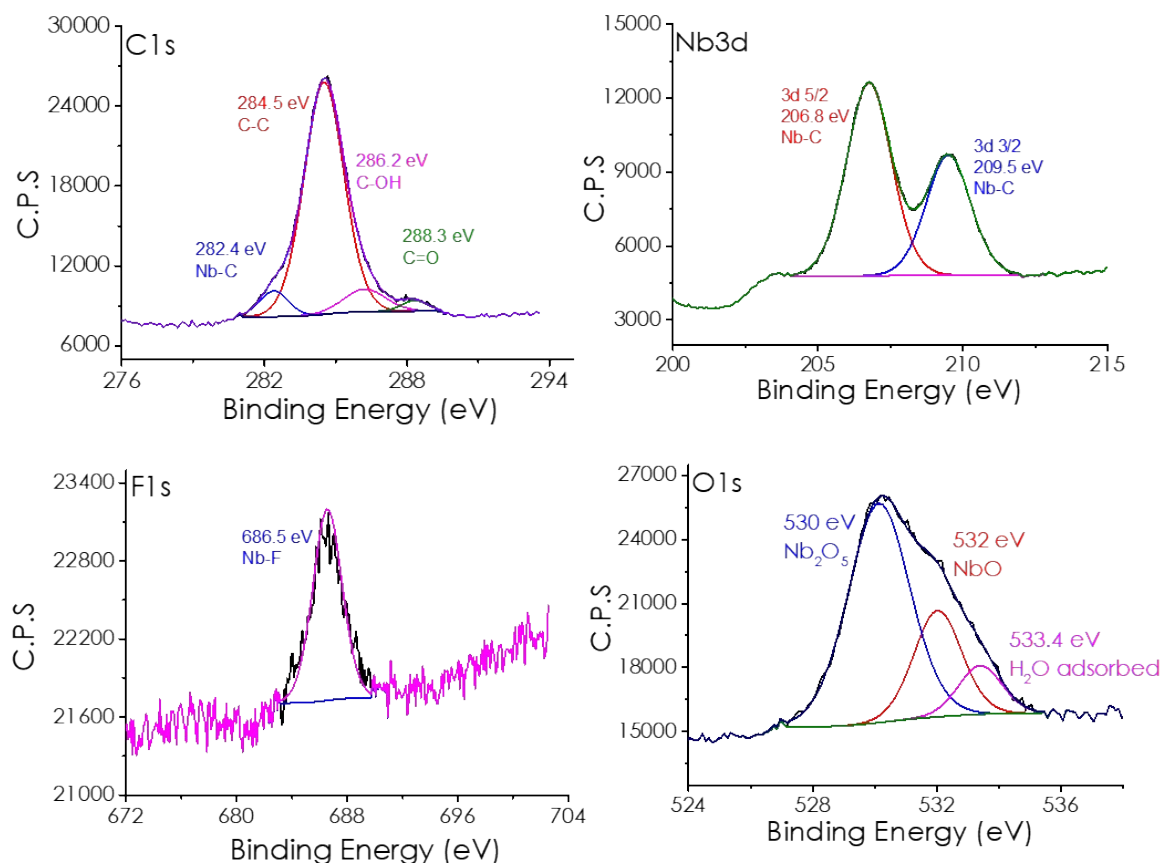


**Fig. S2.** XPS of the Nb<sub>2</sub>C sample after its use as catalyst for the conversion of aniline to azobenzene after consecutive oxidation and hydrogenation.

As will be indicated below, based on experimental information, we have considered that the active sites in the catalyst will be two oxygen vacancies. In the mechanism considered here, molecular oxygen employed as reactant will play the role of refilling the oxygen vacancies and produce two water molecules so that the vacancies are regenerated. Also, adsorbed molecular oxygen will generate an active O-adsorbed atom that will contribute to increase the reactivity of the adsorbed aniline molecules. The overall steps of the reaction are included in Figure S2. A similar mechanism has been proposed in a previous study<sup>i</sup>, with azobenzene and derivatives formed in basic conditions using O<sub>2</sub> as oxidant.

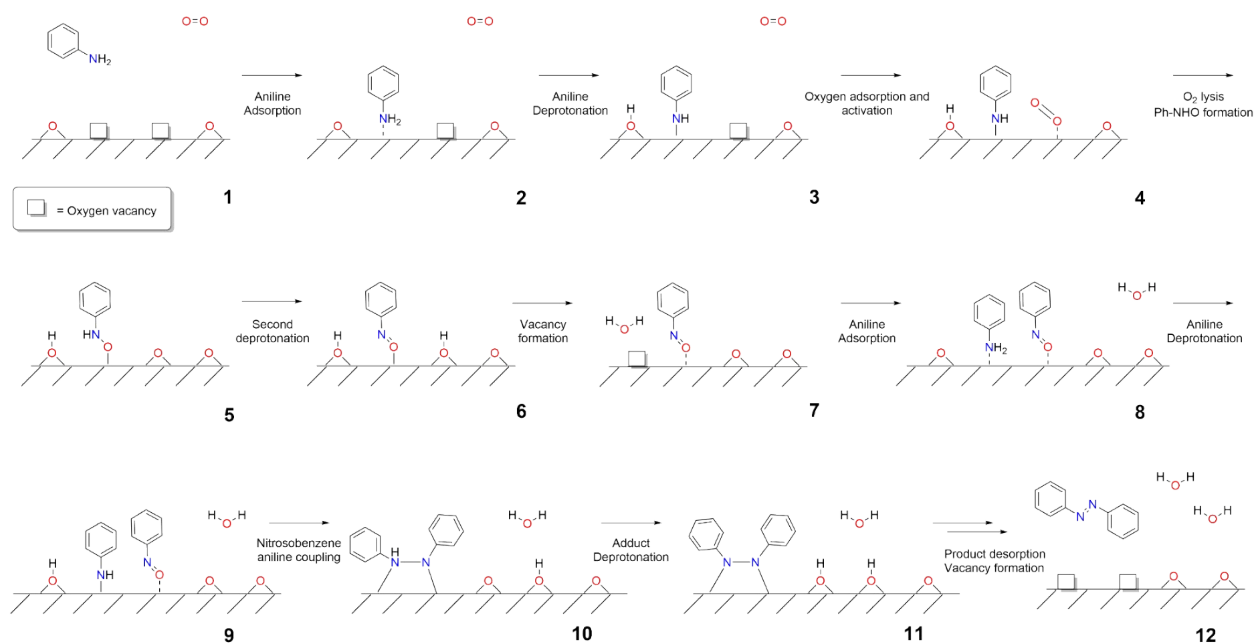


**Figure S3.** Proposed reaction mechanism for the aniline coupling in Nb<sub>2</sub>CO<sub>2</sub> MXene to give azobenzene, with O<sub>2</sub> as oxidant.

### Computational methods.

Two complementary periodic computational methods were employed in this study using Matlantis and CASTEP software respectively. The latter is based on periodic DFT which is well established in the last few decades as a reliable computational tool to explore chemical reactivity in solids.<sup>ii</sup> Matlantis, on the other hand, is a recently presented force field-based software with almost DFT-accuracy and about three orders of magnitude faster in computer time. The idea throughout this computational study is to provide geometry optimized coordinates of the different reaction steps using both Matlantis and CASTEP, in order to determine the best geometries for the reaction coordinate. The structures were optimized using both methods, and re-optimized with the other method, in order to gain more insight of the energy profile and find the true global minima.

### CASTEP

Periodic DFT calculations were conducted using the Cambridge Serial Total Energy Package (CASTEP) module<sup>iii</sup> with the exchange-correlation functional described by Perdew-Burke-Ernzerhof (revised version for solids) within the generalized gradient approximation (GGA-PBEsol).<sup>iv</sup> Tkatchenko and Scheffler (TS) dispersion corrections scheme<sup>v</sup> are incorporated along with the exchange and correlation functional to improve the structural and vibrational properties. Slabs were separated by 20 Å along [001], perpendicular to the surface. A self-consistent field method (tolerance  $5.0 \times 10^{-7}$  eV/atom) was employed in conjunction with plane-wave basis sets with cutoff energy of 500 eV in reciprocal space. All structures are geometry-optimized until energy is converged to  $5.0 \times 10^{-6}$  eV/atom, maximum force to 0.050 eV/Å and maximum displacement to  $5.0 \times 10^{-3}$  Å. The calculations were carried out on Intel Xeon Gold 6248R processors, using 16 cores and 3 GB RAM (DDR4, 2933 MHz) per core. The geometry optimization calculations took on average 72 hours to complete in, on average, 140 cycles.

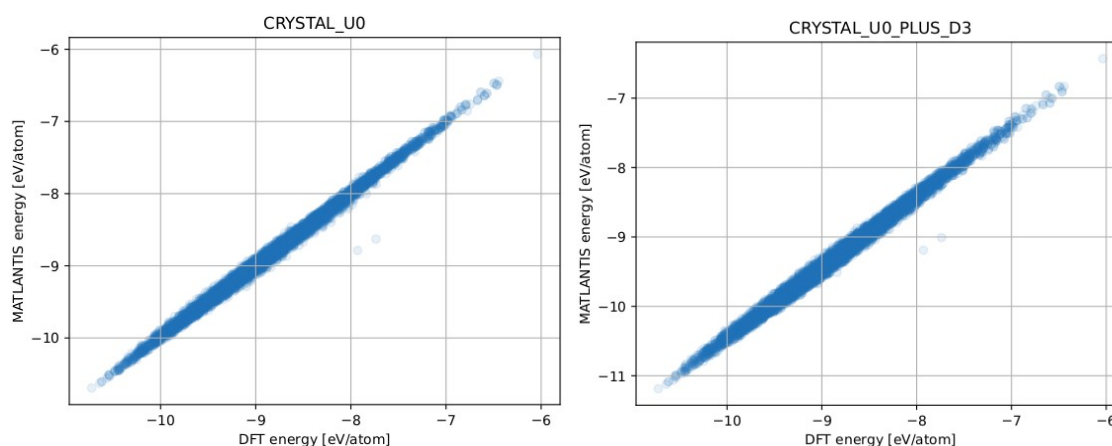
## Matlantis

Since Matlantis is a recently presented software, an initial benchmark has been performed in order to test its accuracy to reproduce energies and geometries of MXene solids. For the benchmark a total of 8590 MAX phase structures were optimized leaving the cell parameters fixed. The structures were taken from Nykiel and Strachan<sup>vi</sup>. First a single point energy calculation was performed on DFT optimized structures and then the resulting energy compared with the one given by DFT. Then, the MAX phase structures were optimized leaving the cell parameters fixed, then atom positions within the cell were fixed and cell parameters were left to relax, in accordance with the methodology in the source paper. For these two calculations the model “CRYSTAL U0” was used. This model was trained on DFT data with the Hubbard parameter set to 0. Lastly a different model in which we are interested was also tested, following the same method as the second calculation. This model is “CRYSTAL U0 PLUS D3”, which was trained on DFT calculations with Hubbard parameter set to 0, but includes D3 dispersion correction. The evaluation metrics were the Mean Average Error (MAE), giving an idea of the expected deviation in energy, and Root Mean Square Error (RMSE), giving an idea of how disperse the errors are, of the energies given by Matlantis and DFT. Numerical results of these tests can be seen on Table S1 and Figure S3.

**Table S1.** Mean Average Error (MAE) and Root Mean Square Error (RMSE) for the comparison between Matlantis and periodic DFT. “CRYSTAL U0 SP” stands for the single point energy calculation without optimization, “CRYSTAL U0” includes geometry optimization and “CRYSTAL U0 + D3” includes D3 dispersion correction and geometry optimization.

Matlantis algorithm	MAE [eV/atom]	RMSE [eV/atom]
CRYSTAL U0 SP	0.0352	0.0020
CRYSTAL U0	0.0353	0.0022
CRYSTAL U0 + D3	0.4407	0.1983

A:



B:

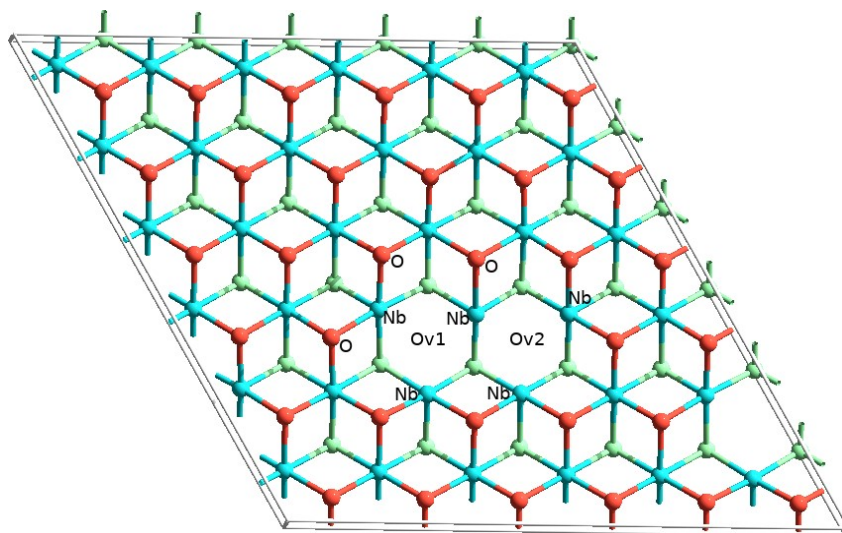


**Figure S4.** A: Calculated energy of MAX phases using Matlantis and DFT. Matlantis algorithms used were CRYSTAL\_U0 (left) and CRYSTAL\_U0+D3 (right). B: Unit cell of  $\text{Nb}_2\text{CO}_2$  MXene with two oxygen vacancies (Ov) employed in the calculations and location in which the different reaction steps take place. ‘Nb’ are the niobium atoms undercoordinated by the presence of the oxygen vacancies. ‘O’ are the oxygen atoms in which hydrogens from aniline are attached, with two such centres producing a water molecule leaving a new oxygen vacancy. Colour code: Nb (blue), O (red), C (light green).

Both single point energy calculation and geometry optimization show good agreement with DFT calculations, with a MAE of just  $\sim 0.035$  eV/atom and a RMSE of  $\sim 0.002$  eV/atom.

Using the D3 dispersion correction model induces higher errors due to the fact that the original DFT calculation of the database did not include this correction. It was nonetheless interesting for us as it is our model of choice for the rest of the calculations in this report, being the most similar to our CASTEP calculations.

The only two outliers are structures ‘6851’ ( $\text{V}_4\text{Mn}_4\text{Ge}_2\text{C}_6$ ) and ‘7966’ ( $\text{V}_4\text{Mn}_4\text{P}_2\text{C}_6$ ) which present an energy difference per atom of 0.8926 and 0.8590 eV/atom. The structure with the next highest energy difference is structure 4096 ( $\text{Mo}_4\text{S}_2\text{N}_2$ ) with 0.1892 eV/atom. The particular details of the  $\text{Nb}_2\text{CO}_2$  MXene will be analyzed later.

Considering very satisfactory the accuracy of Matlantis for the energy and geometry of MAX phases, we include here the technical details of the algorithms used for the study of the aniline coupling reaction. Calculations are carried out with the Neural Network Potential called PreFerreD Potential (PFP)<sup>vii</sup> version 1.14.0 on Matlantis<sup>viii</sup>. From the models offered in Matlantis for the estimator class we chose “CRYSTAL U0 PLUS D3”. This estimator has been trained with no Hubbard parameter and includes D3 dispersion correction. The default option in Matlantis is that force rather than energy is minimized.

For the geometry optimization the Broyden–Fletcher–Goldfarb–Shanno (BFGS) algorithm was used. The convergence condition is a maximum modulus of the forces of 0.05 eV/atom, as suggested on Matlantis documentation. This optimization was performed on atom positions only, with cell parameters being fixed in order to correctly compare with CASTEP. Periodic boundary conditions were applied and a sufficiently large vacuum above and below the MXene ensured no interactions on the z-axis.

### Computational models.

The MXene has the composition  $\text{Nb}_2\text{C}$  and its geometry was taken from the corresponding MAX phase (Materials Project database<sup>x</sup>) with cell parameters  $a=b=3.122$  Å. From this, the Al layer was removed mimicking the experimental etched-based synthesis procedure, and a  $6\times 6$  resulting supercell was considered. The resulting surface (perpendicular to [001]) containing exposed Nb atoms was fully saturated with oxygen atoms, resulting in a final stoichiometry of  $36 \text{Nb}_2\text{CO}_2$ , with unit cell parameters  $a=b=18.735$  Å. It is well known that oxygen vacancies are typically considered as catalytic active sites owing to their ability to facilitate electron transfer and create unsaturated coordination environments that are highly reactive.<sup>x</sup> The oxygen termination on the surface of the MXenes could be removed to form vacancies during the synthesis process or heat treatment.<sup>xi</sup> Thus, we generated two oxygen vacancies, resulting in a unit cell with 178 atoms, according to our suggestion in the mechanism that these two oxygen vacancies are the active sites for the aniline coupling reaction to give azobenzene. Along the [001] direction, the thickness of the MXene is 4.7 Å, and we have added sufficient vacuum ( $c=22.50$  Å in CASTEP and  $c=34.78$  Å in Matlantis) so that the reactions can take place, including all adsorption and desorption processes.

An overview of the unit cell surface and the active sites (oxygen vacancies), as well as the regions of the surface in which the different reaction steps happen is included in Figure S4.

### Computational results.

#### 1. Geometry optimization of $\text{Nb}_2\text{CO}_2$ MXene.

The main results are summarized in Table S2. Both methods show very close Nb-O distance values, with the largest difference being only 0.026 Å. The general trend is that Matlantis Nb-O bond distance tends to be slightly longer than that calculated by CASTEP. This means that Matlantis found CASTEP optimized structures to be systematically above the minimum by three to four eV, with very similar final geometries.

**Table S2.** Bond distances (Å) in optimized  $\text{Nb}_2\text{C}$  MXene using CASTEP and Matlantis, compared with the values from Materials Project.

	CASTEP	Matlantis	Materials Project
Nb-Nb same layer	3.12	3.17	3.15
Nb-Nb different layer	2.93	2.99	3.08
C-Nb	2.14	2.18	2.21

## 2. Geometry optimization of all the reaction steps of the aniline coupling.

The main details of each step will be given below. Full geometries are given as CIF files in Supporting Information. The resulting energy reaction paths with Matlantis and CASTEP are shown in Figures S5 and S6 respectively. Figures of the geometries of all steps are given below. All steps are numbered according to the mechanism indicated in Figure S2.

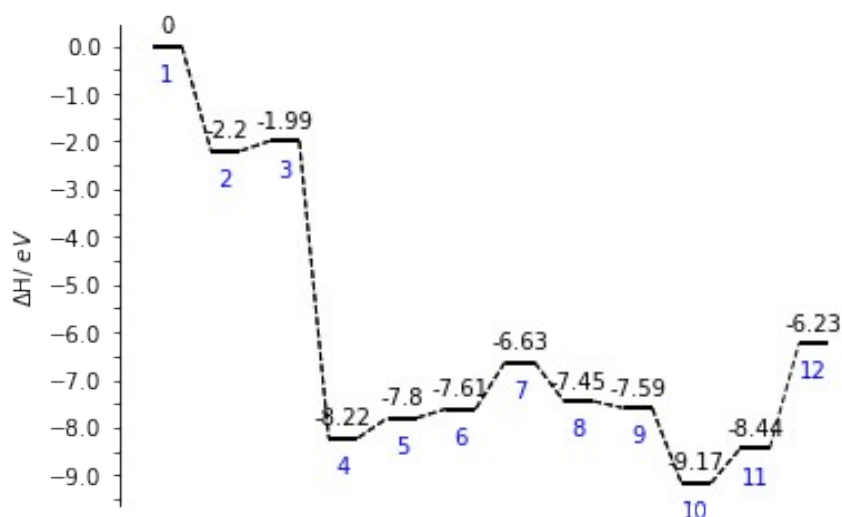


**Figure S5:** CASTEP calculated energy profile of the reaction path. All steps are numbered according to the mechanism indicated in Figure S1.

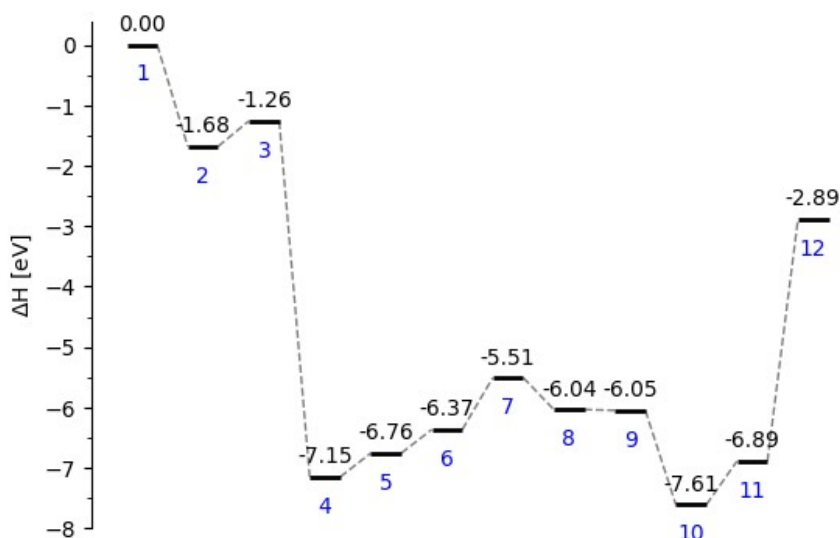


**Figure S6:** Matlantis calculated energy profile of the reaction path. All steps are numbered according to the mechanism indicated in Figure S1.

Step 1. This is just the initial configuration with one aniline and an oxygen molecule relatively far from the catalyst surface, hence without any adsorption taking place.

Step 2. Aniline adsorbs on one of the oxygen vacancies. Due to the presence of two oxygen vacancies, 6 Nb atoms (3 per O vacancy) are undercoordinated and accessible for adsorption. A N-Nb interaction (2.40 Å in Matlantis and 2.66 Å in CASTEP) appears when aniline is adsorbed. The adsorption energies are -1.68 eV (Matlantis) and -2.2 eV (CASTEP).

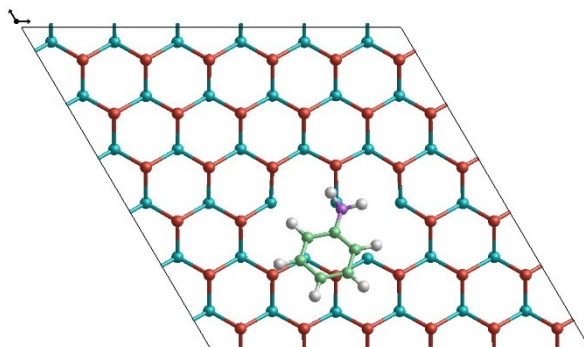


**Figure S7.** Step 2. Aniline is adsorbed in one of the two oxygen vacancies of Nb<sub>2</sub>CO<sub>2</sub> MXene. N-Nb distance is 2.40 Å in Matlantis and 2.66 Å in CASTEP.

Step 3. A hydrogen atom in NH<sub>2</sub> detaches from aniline, forming an OH termination group on the MXene surface. Two N-Nb bonds form with lengths 2.27 Å and 2.39 Å. Ph-NH rotates so that the phenyl group lies sideways on the adjacent oxygen vacancy. Mulliken Charge analysis (Table S3) shows that charge transferred from aniline to Nb<sub>2</sub>CO<sub>2</sub> Mxene is -0.274.

**Table S3.** Mulliken Charge distribution of free aniline (Step 1), adsorbed aniline (Step 2), and dehydrogenated aniline (Step 3). Atoms bonded to N are C4, H6, H7. Atom transferred to Nb<sub>2</sub>CO<sub>2</sub> Mxene in Step 3 is H7, marked with an asterisk.

Atom No.	Aniline Charge (e)	AdsorbedAniline Charge (e)	Dehydrogenated Aniline Charge (e)
H1	0.281	0.231	0.237
H2	0.302	0.311	0.317
H3	0.296	0.309	0.308
H4	0.302	0.254	0.218
H5	0.281	0.132	0.069
H6	0.447	0.341	0.309
H7	0.448	0.347	0.419*
C1	-0.327	-0.305	-0.306
C2	-0.298	-0.275	-0.268
C3	-0.331	-0.303	-0.35
C4	0.139	0.04	0.034
C5	-0.331	-0.297	-0.291
C6	-0.298	-0.294	-0.295
N	-0.911	-0.765	-0.734
Sum	0	-0.274	-0.333

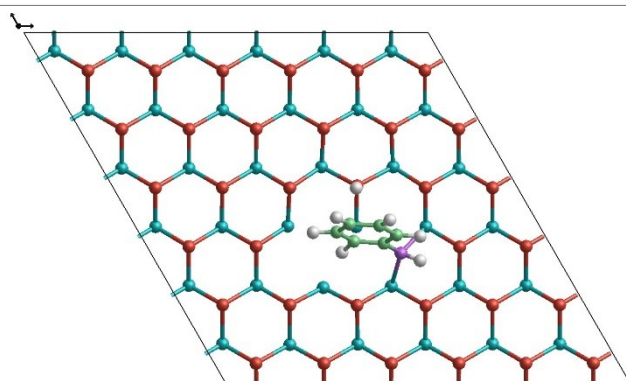


**Figure S8.** Step 3. A hydrogen atom in  $\text{NH}_2$  detaches from aniline, forming an OH termination group on the MXene surface, with Ph-NH forming two N-Nb bonds.

Step 4. An oxygen molecule adsorbs on the adjacent O-vacancy, activating the  $\text{O}=\text{O}$  bond, which elongates from the original distance, 1.24 Å, to 2.28 Å. One of the oxygens fills the vacancy still left on the surface while the other remains interstitial between oxygen termination groups close to the adsorbed Ph-NH, with a  $\text{O}\cdots\text{H}$  distance of 2.24 Å.

CASTEP and Matlantis geometries differ in the way the  $\text{O}_2$  molecule fills the oxygen vacancy, with the common description that one of these two oxygens locates in the oxygen vacancy. Whilst in CASTEP the second oxygen protrudes outside keeping an elongated  $\text{O}_2$  chemisorbed molecule, “ready” for the following coupling reaction, in Matlantis the  $\text{O}=\text{O}$  bond is fully broken and the second oxygen approaches the other oxygen vacancy, partially blocked by the adsorbed Ph-NH, but also preparing the next step in which a N-O bond is formed. This leads to the CASTEP geometry being  $\sim 2.5$  eV less stable, since the second oxygen is still not interacting with undercoordinated Nb atoms of the oxygen vacancy partially occupied by adsorbed Ph-NH.

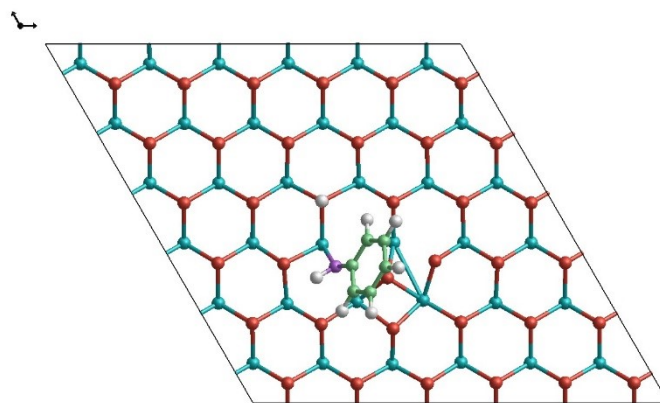


**Figure S9.** Step 4. An oxygen molecule is adsorbed on the oxygen vacancy adjacent to the adsorbed Ph-NH.

Step 5. The second oxygen from the adsorbed  $O_2$  interacts with the adsorbed Ph-NH, generating a N-O bond leading to the adsorbed Ph-NHO intermediate, with distance O-N 1.44 Å, and two O-Nb distances of 2.24 Å. N remains coordinated to a Nb atom with a N-Nb distance of 2.31 Å. N-Nb and N-O distances are practically the same in CASTEP and Matlantis.

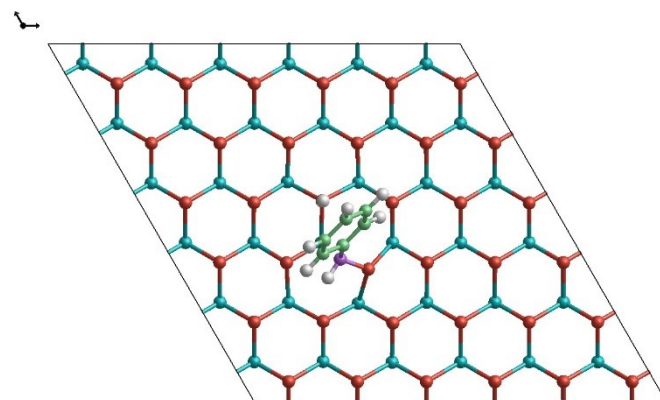


**Figure S10.** Step 5. Oxygen from the adsorbed  $O_2$  interacts with the adsorbed Ph-NH, generating the adsorbed Ph-NHO intermediate.

Step 6. Nitrosobenzene is formed by hydrogen transfer of the Ph-NHO intermediate on the MXene surface, creating a second OH termination group on the MXene surface plus adsorbed Ph-NO. N-Nb distance is 2.19 Å, and two O-Nb distances are 2.19 Å and 2.12 Å. Matlantis and CASTEP geometries are identical. Hence, the previous differences found in Step 5 regarding the  $O_2$  chemisorption indicates just a difference in when the O=O breaks and the second oxygen migrates to the second oxygen vacancy.

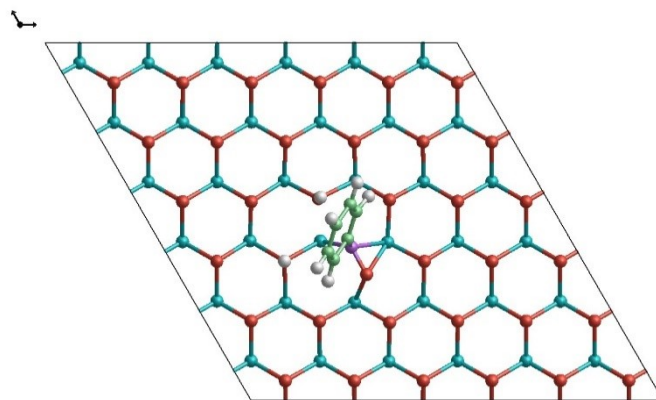


**Figure S11.** Step 6. Adsorbed Ph-NO is formed by hydrogen transfer of Ph-NHO to the MXene surface, creating a second OH group.

Step 7. Two neighbor OH groups form a water molecule and regenerate one of the oxygen vacancies. Related to this, direct hydrogen migration (diffusion) through the many available surface oxygens has been studied, and an energy barrier of 2.02 eV has been found using Matlantis. However, the same process following a Grotthuss-style mechanism (water assisted H migration) presents a barrier of only 0.10 eV. The water formed remains adsorbed on the vacancy and therefore an additional energy contribution of 0.62 eV on Matlantis is necessary in order to leave the site free for the next steps. The geometries found by CASTEP and Matlantis were practically the same, with a minimum difference in the orientation of the adsorbed water molecule with respect to the catalyst surface.

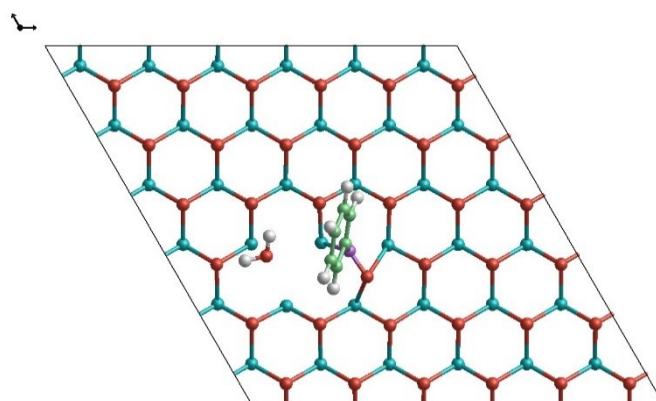


**Figure S12.** Step 7. Water formation through condensation from two neighbor OH groups.

Step 8. The second aniline molecule adsorbs on the oxygen vacancy just created, leading to an interaction with the nitrosobenzene Ph-NO moiety. The N-Nb distance is 2.46 Å, similar (2.34 Å) to that found in the first aniline adsorption, but slightly longer. Matlantis and CASTEP reached very similar structures, with Matlantis energy differing only 0.1 eV from CASTEP.

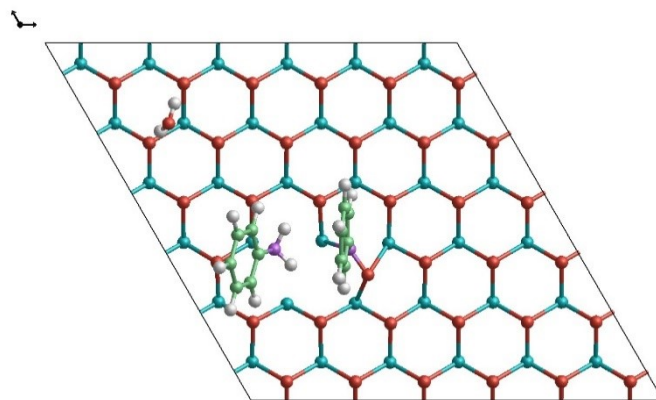


**Figure S13.** Step 8. Adsorption of the second aniline molecule on oxygen vacancy leading to adsorbed Ph-NH<sub>2</sub> interacting with Ph-NO.

Step 9. The adsorbed aniline donates a proton to the MXene surface, forming a surface OH in a similar way to Step 3. The two formed aniline N-Nb bonds are 2.27 Å and 2.39 Å, similarly to the ones in Step 3 with identical values. The hydrogen on the NH is at a distance of 2.20 Å from the nitrogen in the adsorbed nitrosobenzene. This small distance indicates the convenience of the geometry of the two adsorbed anilines with respect to the coupling reaction. Matlantis and CASTEP gave very similar geometries, with energies differing by only 0.1 eV.

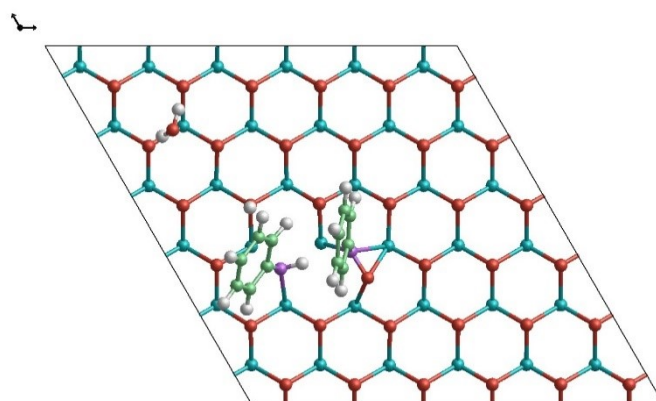


**Figure S14.** Step 9. The second aniline adsorbed donates a proton to the MXene surface, forming a surface OH.

Step 10. Ph-NO is coupled with Ph-NH, generating a N-N bond with distance 1.46 Å, while breaking the N-O bond. This oxygen is then fully coordinated to the surface, completely filling the oxygen vacancy on which the Ph-NHO intermediate was adsorbed. The adsorbed Ph-NHN-Ph moves to occupy the other oxygen vacancy where the second aniline adsorbed. There are three N-Nb bonds, 2.41 Å and 2.34 Å belonging to the fully deprotonated hydrogen, and the other one 2.37 Å. Matlantis and CASTEP gave very similar geometries, with energies differing by only 0.1 eV.

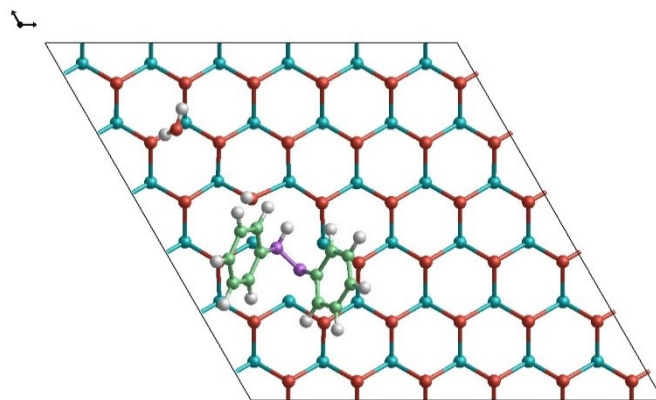


**Figure S15.** Step 10. Formation of Ph-NHN-Ph (N-N bond).

Step 11. Hydrogen from Ph-NHN-Ph migrates to the surface forming an OH group, contributing to strengthening the N-N bond, whose distance becomes 1.42 Å. The single N-Nb bond distance is reduced from 2.37 Å to 2.15 Å.

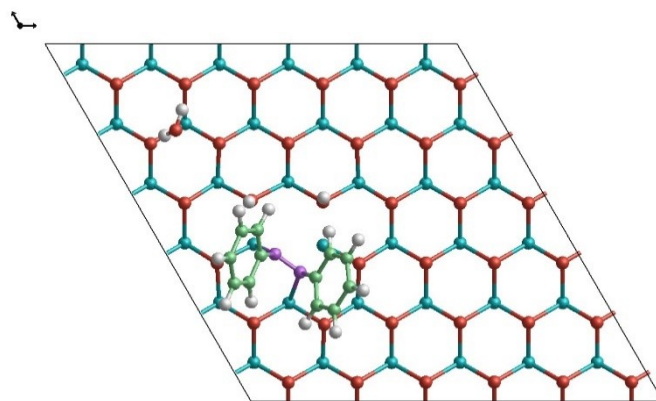


**Figure S16.** Step 11. Dehydrogenation of Ph-NHN-Ph and formation of adsorbed azobenzene.

Step 12. Azobenzene is desorbed from the surface in its relatively unstable *cis* conformation, as formed from the previous step, leading to the *trans*-azobenzene product upon non-radiative relaxation process<sup>xiii</sup>, and restoring an oxygen vacancy. From the remaining two OH surface groups, water can be formed in a similar way to Step 7, regenerating the second oxygen vacancy. Using Matlantis, desorption of azobenzene in its bent configuration results in an energy of 3.01 eV, and then a reoptimization to the more stable ‘*trans*’ conformation contributes to an additional 0.61 eV energy stabilization. Adding an energy of about 0.86 eV for water formation, plus about 0.74 eV for water desorption results in an overall energy change from Step 11 to Step 12 of about 4.0 eV, as can be seen in Figure S6.

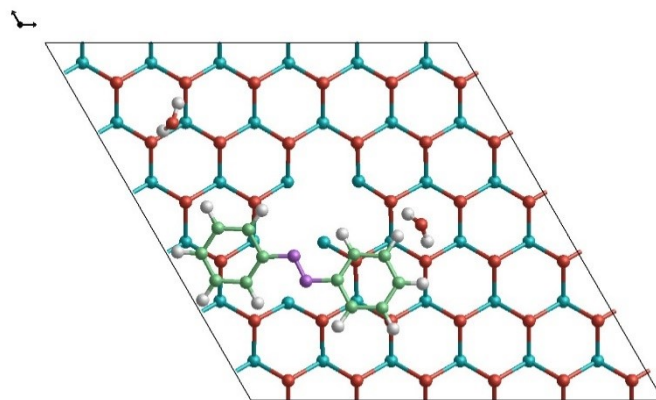


**Figure S17.** Step 12. Azobenzene desorption and water formation to regenerate the two initial oxygen vacancies.

Steps 11 and 12 show some differences between Matlantis and CASTEP, but they are due to Matlantis reaching in advance the final step. This is very similar to what was found in Steps 4 and 5 in which Matlantis found simultaneously the adsorption and dissociation of the  $O_2$  molecule whilst CASTEP found the same result in two subsequent steps. Here again, CASTEP is describing the desorption and reconfiguration (from cis to trans) of azobenzene in two steps whilst Matlantis is reaching the same result in only one step. Probably Matlantis algorithm for geometry optimization is analyzing a larger region outside the current geometry.

### 3. Synergy between Matlantis and CASTEP.

A synergistic and iterative calculation process has been carried out in order to get the best possible outcome of the reaction structures with both Matlantis and CASTEP software. Thanks to Matlantis speed and wider geometry-optimization range, it could usually explore a wider range of possible geometrical configurations, which we used to explore more plausible reaction pathways that would be extremely time-consuming in CASTEP. This allowed us to compare results from Matlantis and CASTEP, usually confirming the minima found. One example of this would be step 2, the first aniline adsorption. The geometries can be seen on Figure S18.

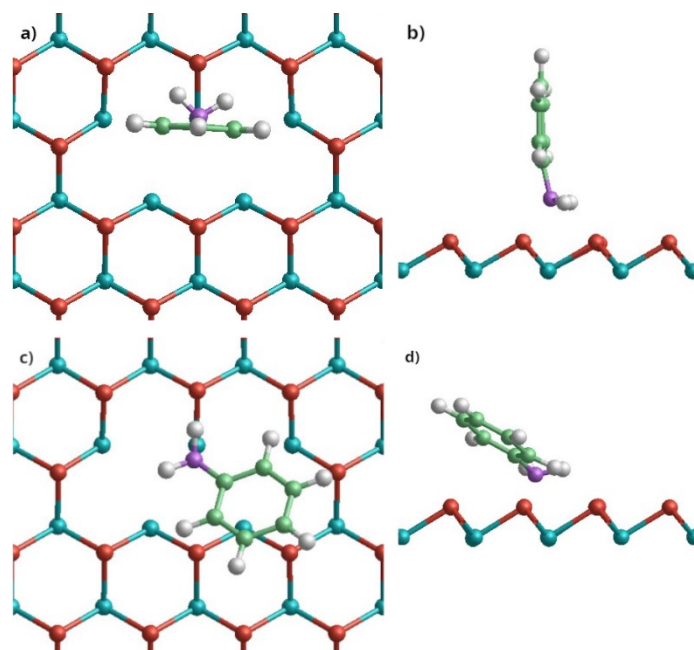


**Figure S18.** Step 2. Geometry from CASTEP (a,b), xy-view (a) and xz-view (b). Geometry from Matlantis (c,d), xy-view (c) and xz-view (d).

On this intermediate, CASTEP optimized the structure until the N-Nb distance was 2.66 Å. Matlantis however shortened this distance to 2.39 Å, drastically changing the geometry and resulting in a lower energy configuration by 1.36 eV.

On structures 5-8, the structures found by both methods, while having slight differences, are geometrically very similar and do not show significant energy differences.

On the other hand, on structures 10 to 12, CASTEP did not find the minima of the fully adsorbed intermediate, instead reaching an intermediate geometry, i.e. local minima that were not fully adsorbed. On structure 10, azobenzene remained adsorbed through only one N (the one from previous Ph-NO intermediate), with a distance N-Nb of 2.91 Å.

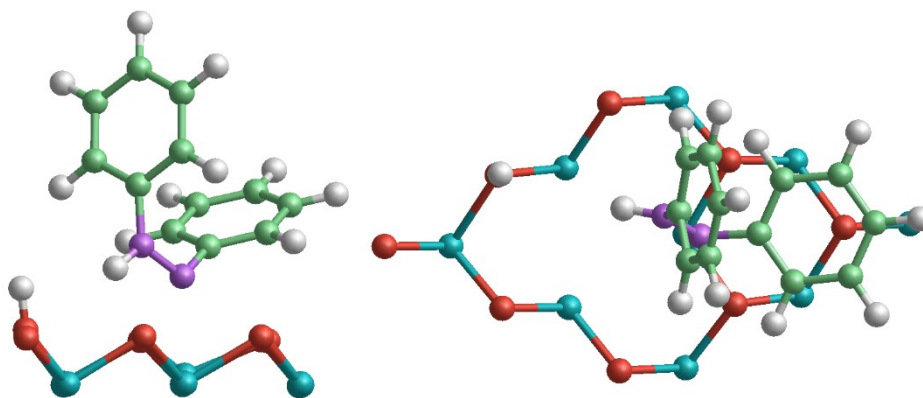


**Figure S19.** Side (left) and top (right) views of CASTEP-optimized Step 10.

This same structure re-optimized in Matlantis yields the same intermediate adsorbed through both N atoms, being the Ph-NO coordinated to 2 Nb atoms, with distances N-Nb of 2.26 and 2.34 Å, while the other N is bonded to another Nb with a distance N-Nb of 2.31 Å.

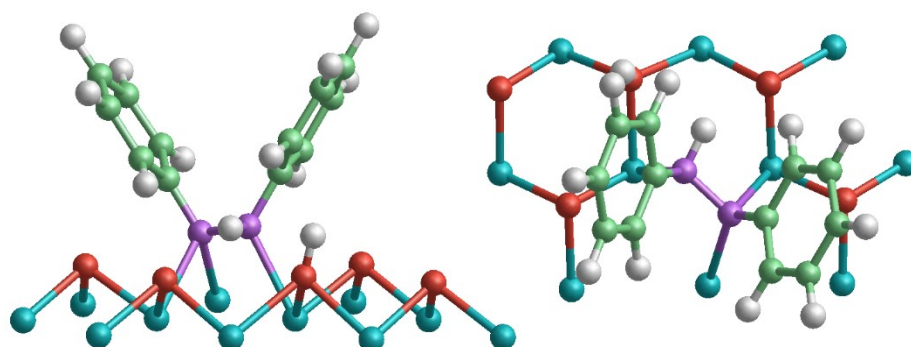


**Figure S20.** Side (left) and top (right) views of Matlantis→CASTEP-optimized Step 10.

A similar behavior is shown when optimizing intermediate 11. On CASTEP, deprotonation and vacancy formation seem to occur in a single step (combining 10 and 11), as the deprotonation appears to happen directly on an already H-containing O surface group, yielding H<sub>2</sub>O and desorbing the product. Intermediate 11 provided by CASTEP was then optimized in Matlantis, and it found a different geometry in which the azobenzene remains strongly adsorbed, rather than the original geometry weakly adsorbed through only one N-Nb bond. The main difference is the stronger adsorption of the reaction product by Matlantis, which leads in the last step to the high desorption energy. CASTEP on the other hand predicts a weaker adsorption for azobenzene.

The use in Matlantis of other optimizers, such as FIRE<sup>xiii</sup> and FIRELBFGS (a combination of FIRE and LBFGS offered by Matlantis), seems promising in finding the same intermediate minima than CASTEP.

### Synergy conclusions

We have compared and iteratively used both Matlantis and CASTEP results in order to gather the best possible results. In general terms, we found Matlantis to be capable of finding lower energy minima, which CASTEP confirmed as true minima. Only using CASTEP often resulted in energies stuck on local minima. However, Matlantis was unable to find some less stable local minima that CASTEP was able to find.

---

<sup>i</sup> S. Takamoto, C. Shinagawa, D. Motoki, K. Nakago, W. Li, I. Kurata, T. Watanabe, Y. Yayama, H. Iriguchi, Y. Asano, T. Onodera, T. Ishii, T. Kudo, H. Ono, R. Sawada, R. Ishitani, M. Ong, T. Yamaguchi, T. Kataoka, A. Hayashi, N. Charoenphakdee and T. Ibuka, Towards universal neural network potential for material

- 
- discovery applicable to arbitrary combination of 45 elements. *Nature Commun.* 2022, **13**, 2991. <https://doi.org/10.1038/s41467-022-30687-9>
- ii *Matlantis*, software as a service style material discovery tool <https://matlantis.com/>.
- iii A. Jain, S. P. Ong, G. Hautier, W. Chen, W. D. Richards, S. Dacek, S. Cholia, D. Gunter, D. Skinner, G. Ceder and K. A. Persson, Commentary: The Materials Project: A materials genome approach to accelerating materials innovation. *APL Matter.* 2013, **1**, 011002. <https://doi.org/10.1063/1.4812323>
- iv Segall MD, Lindan PJD, Probert MJ, Pickard CJ, Hasnip PJ, Clark SJ, Payne MC. First-principles simulation: ideas, illustrations and the CASTEP code. *J. Phys.-Condes. Matter.* 2002; **14**: 2717-2744.
- v Perdew J P, Ruzsinszky A, Csonka G I, Vydrov O A, Scuseria G E, Constantin L A, Zhou X, Burke K . Restoring the density-gradient expansion for exchange in solids and surfaces. *Phys. Rev. Lett.* 2008, **100**(13): 136406.
- vi Tkatchenko A, Scheffler M. Accurate molecular van der Waals interactions from ground-state electron density and free-atom reference data. *Phys. Rev. Lett.* 2009, **102**(7): 073005.
- vii Rombouts, J. A.; Ehlers, A. W.; Lammertsma, K. A quantitative analysis of light-driven charge transfer processes using voronoi partitioning of time dependent DFT-derived electron densities. *Journal of Computational Chemistry* 2017, **38** (20), 1811–1818. <https://doi.org/10.1002/jcc.24822>.
- viii K. Nykiel and A. Strachan, High-throughput density functional theory screening of double transition metal MXene precursors. *Scientific Data*, 2023, **10**, 827. <https://doi.org/10.1038/s41597-023-02755-2>.
- ix Konaka, R.; Kuruma, K.; Terabe, S. Mechanisms of oxidation of aniline and related compounds in basic solution. *Journal of the American Chemical Society* 1968, **90** (7), 1801–1806. <https://doi.org/10.1021/ja01009a022>.
- x Chen B W J, Xu L, Mavrikakis M. Computational methods in heterogeneous catalysis. *Chem. Rev.* 2020, **121**(2): 1007-1048.
- xi Hou T, Luo Q, Li Q, Zu H, Cui P, Chen S, Lin Y, Chen J, Zheng X, Zhu W, Liang S, Yang J, Wang L . Modulating oxygen coverage of Ti<sub>3</sub>C<sub>2</sub>T<sub>x</sub> MXenes to boost catalytic activity for HCOOH dehydrogenation. *Nature Commun.* 2020, **11**(1), 4251.
- xii Chung C H, Tu F Y, Chiu T A, Wu T T, Yu W Y. Critical roles of surface oxygen vacancy in heterogeneous catalysis over ceria-based materials: A selected review. *Chem. Lett.*, 2021, **50**(5), 856-865.
- xiii E. Bitzek, P. Koskinen, F. Gähler, M. Moseler and P. Gumbsch, Structural Relaxation Made Simple. *Phys. Rev. Lett.*, 2006, **97**, 170201. <https://doi.org/10.1103/PhysRevLett.97.170201>.